Nano Research
2023, 16(2): 3125–3129

ISSN 1998-0124 CN 11-5974/O4
https://doi.org/10.1007/s12274-022-4968-0

Communication

Luminescent nanoparticle-arrays synthesized via polymer pen lithography

Ping Wang[1,§], Shuyi Bao[1,§], Shuqian Qiao[2], Ce Li[1], Zhang Jiang[1], Hao Song[1], Yilin Wang[1], Qiuqiang Zhan[2] (✉), and Ling Huang[1,3] (✉)

[1] *Institute of Advanced Materials, Jiangsu National Synergetic Innovation Center for Advanced Materials (SICAM), Nanjing Tech University, Nanjing 211816, China*
[2] *Centre for Optical and Electromagnetic Research, Guangdong Provincial Key Laboratory of Optical Information Materials and Technology, National Centre for International Research on Green Optoelectronics, South China Academy of Advanced Optoelectronics, South China Normal University, Guangzhou 510006, China*
[3] *College of Chemistry, State Key Laboratory of the Chemistry and Utilization of Carbon Based Energies, Xinjiang University, Urumqi 830046, China*
[§] *Ping Wang and Shuyi Bao contributed equally to this work.*

Received: 3 August 2022 / **Revised:** 25 August 2022 / **Accepted:** 25 August 2022

ABSTRACT

We report a high-throughput approach to generating lanthanide-doped upconversion nanoparticle (UCNP) arrays through polymer pen lithography (PPL), where instead of the expensive block co-polymer, two types of polymers are employed with one working as ink carrier, e.g., polyethylene glycol-400 (PEG-400) to facilitate smooth transfer from the tip to the substrate and the other, e.g., polyvinyl pyrrolidone (PVP), as chelator to ensure successful patterning of metal ions. The strong coordination of PVP with rare earth ions (RE^{3+}) is the key for weakening the interaction between RE^{3+} ions and the carrier PEG-400 so that the good mobility of ink can be retained. Further experimental results have shown that besides PVP, small molecules with functional groups that can coordinate with RE^{3+} ions, such as oleic acid, can also serve the same role as PVP, which greatly enriches the ink library for PPL. Over 1 cm^2 area arrays comprising individual UCNP can be reliably generated with characteristic upconversion luminescence. This strategy not only allows reliable production of individual UCNP arrays, it also paves new avenue to the precise synthesis of multifunctional NPs for lasing, imaging, encryption, and anticounterfeiting.

KEYWORDS

polymer pen lithography, upconversion luminescence, nanoparticle, array, ligand

1 Introduction

Lanthanide-doped upconversion nanoparticles (UCNPs), with characteristics of high chemical stability, large anti-Stokes shift, widely tunable lifetime, and sharp emission peaks, have attracted increased research enthusiasms in the past decades [1–4], and have been investigated in a broad variety of areas such as display, bioimaging, theranostics, and compact solid-state lasers [5–10]. Moreover, sophisticated control of UCNPs in terms of dimension, phase structure, chemical composition, and morphology, has enabled the very latest advances including single nanoparticle luminescence, Brownian motion tracking of UCNPs [11], advanced anticounterfeiting [12, 13], *in-situ* temperature monitoring [14], optical manipulation of protein subcellular localization in cells [15, 16], optogenetics [17], and solar energy harvesting/conversion [18].

Successful utilization of these luminescent materials requires effective strategies for generating arrays of such UCNPs in an expected manner. Unlike some other lithographic techniques [19–21], as a well-developed technology invented in the year of 1999 [22], dip-pen nanolithography is particularly suitable for producing molecular arrays with arbitrary design and at the nanoscale resolution. Except direct patterning of small molecules [23, 24], employment of polymers as ink carriers has facilitated reliable patterning of different types of nanomaterials ranging from Au nanoparticles with different sizes, to magnetic Fe_3O_4 NPs, fullerene, biomolecules, and conducting polymers [25–28].

Different from the above scenario where there is no chemical interaction between target materials and ink carrier, in the process of patterning noble metal ions, a specially designed di-block copolymer of poly(ethylene oxide)-b-poly(2-vinylpyridine) (PEO-b-P2VP) was employed, with one block working as ink carrier while the other as a ligand coordinated with target metal ions. This ensures both smooth transfer of the ink material from tip to the substrate and meanwhile effective delivery of metal ions through coordination interaction. Therefore, metal ions in such patterned dot arrays will work as nanoreactors where proper control of the coarsening conditions leads to formation of arrays with each pattern comprising one nanoparticle [29, 30]. However, the types of available block co-polymers are very limited and also expensive. In order to simplify this principle and extend the applicable chelators, herein by replacing the block co-polymer with intentionally mixing two kinds of polymers with one working as

Address correspondence to Qiuqiang Zhan, zhanqiuqiang@m.scnu.edu.cn; Ling Huang, iamlhuang@njtech.edu.cn

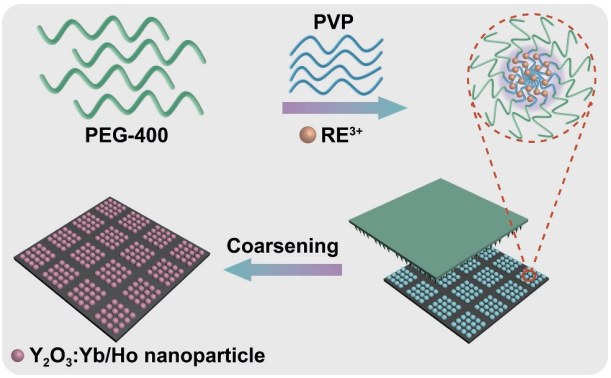

Scheme 1 Schematic illustration of UCNP array generation process through polymer pen lithography.

ink carrier and the other as ligand (Scheme 1), we have for the first time, successfully generated arrays of UCNPs at 100% reproducibility. Further modulation of the coarsening and annealing parameters converts such nanoreactor arrays into individual UCNP arrays, which show typical upconversion luminescence under 980 nm laser excitation.

2 Results and discussion

As shown in Fig. 1(a), rare earth ions (RE^{3+}) are prone to coordinate with the oxygen atoms in polyethylene glycol (PEG), which is utilized as ink carrier. Compared with the ethanol solution containing only PEG, a ~ 18 cm^{-1} Fourier transform infrared (FT-IR) peak offset from 1,100 to 1,082 cm^{-1} corresponding to the ether bond (–C–O–C–) was observed upon addition of RE^{3+} in the solution, which indicates the chemical interaction between PEG and RE^{3+} (Fig. 1(b)). Compared with pure ethanol solution of polyvinyl pyrrolidone (PVP), the carbonyl (–C=O) FT-IR peak of the ink containing both PVP and RE^{3+} shifted from 1,644 to 1,622 cm^{-1} was seen, evidencing again that RE^{3+} ions are coordinated with PVP (Fig. 1(c)). Following this idea, we assume similar coordination interaction to that of the block copolymer PEO-b-P2VP shall occur, when RE^{3+} ions are added into the ink containing both polyethylene glycol-400 (PEG-400) and PVP, that is, PEG-400 works as ink carrier while PVP as ligand coordinates with RE^{3+} ions, so that promoted ink transfer from tip to substrate may be expected (Fig. 1(d)). Different from the clear solution of PEG-400, white precipitate appeared immediately when RE^{3+} was added into the ethanol solution of PVP (Figs. 1(e) and 1(f)), suggesting not only the formation of RE^{3+} complex, but also the stronger coordination capability of PVP than that of PEG-400 [31, 32]. Since the RE^{3+} complexes are insoluble in ethanol, 100 μL/mL of water was added into solution to dissolve the RE^{3+} complex to form a transparent uniform ink for lithography (Fig. 1(g))

Meanwhile, the chemical interaction between the ether bond (–C–O–C–) in PEG chain and RE^{3+} ions causes disorder of the PEG chain and cannot transfer from the tip to the substrate as smoothly as that without RE^{3+}, which makes the polymer pen lithography (PPL) process unfeasible. Indeed, regularly patterned PEG dot arrays can be reliably generated in the absence of RE^{3+} (Figs. 2(a) and 2(b)). However, patterning can hardly work when RE^{3+} ions are added into the ink solution (Figs. 2(c) and 2(d)), and only irregularly patterned dots with uneven sizes can be seen.

As a stark contrast, PEG dot arrays containing RE^{3+} can be reliably obtained once a chelator, PVP, which has stronger coordinating interaction than that of PEG, is added into the ink solution. As large as ~ 1 cm^2 PEG dots arrays containing $Y(NO_3)_3$, $Er(NO_3)_3$, and PVP can be easily generated, where uniform size distribution can be seen in zoomed-in optical images in Figs. 3(a)–3(c), dot arrays covering an area as large as ~ 1 cm^2 can be easily generated and zoomed in optical images show very uniform

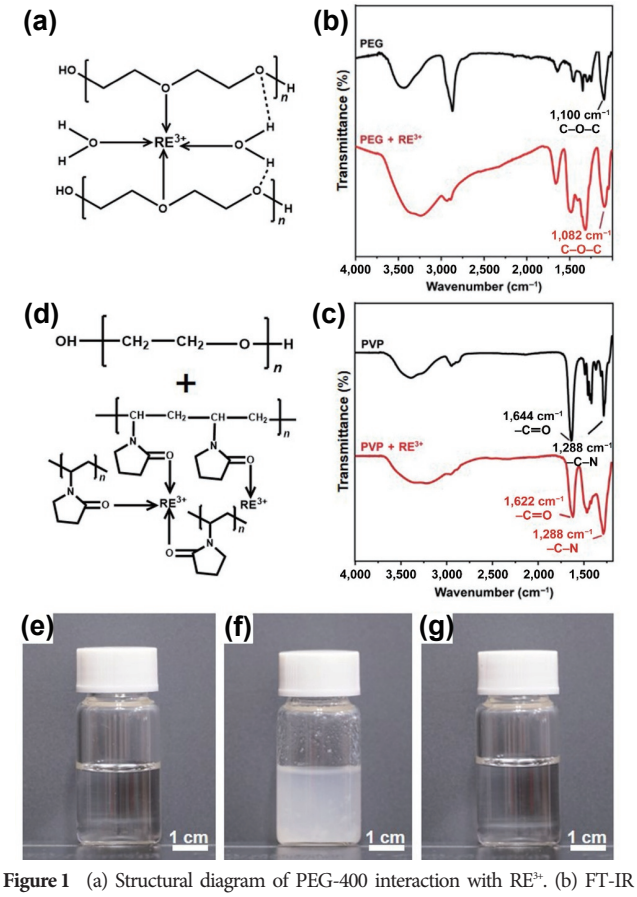

Figure 1 (a) Structural diagram of PEG-400 interaction with RE^{3+}. (b) FT-IR spectra of PEG-400 and the mixture of RE^{3+} with PEG-400. (c) FT-IR spectra of PVP and the mixture of RE^{3+} with PVP. (d) The coordination status of the ink containing PEG-400 and complex between RE^{3+} and PVP. Optical images of (e) PEG-400, (f) mixture of PVP with RE^{3+}, and (g) mixture of PVP with RE^{3+} after addition of 100 μL H_2O per mL in ethanol ink where the white precipitate becomes dissolved.

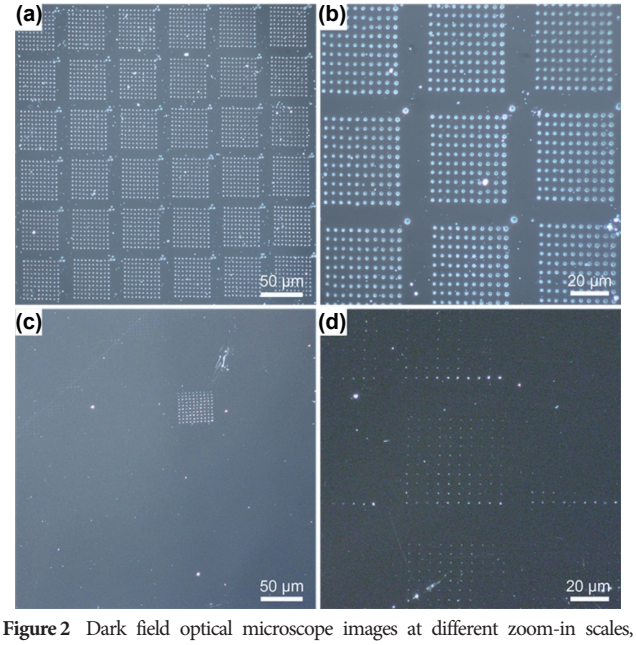

Figure 2 Dark field optical microscope images at different zoom-in scales, showing patterned dot arrays using ((a) and (b)) PEG-400 in ethanol solution and ((c) and (d)) PEG-400 ethanol solution containing RE^{3+}.

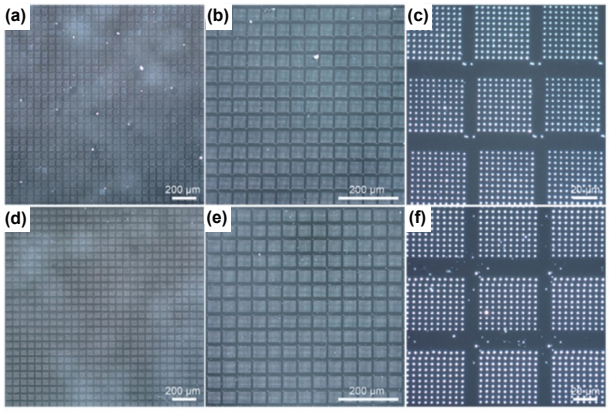

Figure 3 Dark field optical microscope images at different zoom-in scales, showing the patterned dot arrays of PEG-400 in ethanol solution containing (a)–(c) $Y(NO_3)_3$, $Er(NO_3)_3$, and PVP, and (d)–(f) $Y(NO_3)_3$, $Yb(NO_3)_3$, $Ho(NO_3)_3$, and PVP.

size distribution of PEG dots containing $Y(NO_3)_3$, $Er(NO_3)_3$, and PVP. Similarly, such dot arrays containing $Y(NO_3)_3$, $Yb(NO_3)_3$, $Ho(NO_3)_3$, and PVP can also be prepared (Figs. 3(d)–3(f)). Here we would like to emphasize that addition of PVP has successfully weakened the coordination effect between PEG and RE^{3+}, which ensures nearly 100% repeatability of such patterning.

Following this principle, certain amount of a small organic molecule, oleic acid, $C_{17}H_{31}COOH$, which can also form strong coordination bond with RE^{3+}, is introduced to replace PVP. As shown in Figs. S1 and S2 in the Electronic Supplementary Material (ESM), respectively, dot arrays containing $La(CF_3COO)_3$, $Yb(CF_3COO)_3$, $Er(CF_3COO)_3$, as well as $Na(CF_3COO)$, $Yb(CF_3COO)_3$, $Er(CF_3COO)_3$, and $Y(CF_3COO)_3$ are generated with 100% reproducibility.

Our experimental results have further proved that hydrophilicity of the substrate surface is also very critical to ensure successful patterning. Since ethanol is used as solvent for ink preparation and the contact angle of the quartz wafer's surface (after cleaning with isopropanol, ethanol, and acetone) is in the range of 40°–50° (Fig. 4(a)). Therefore, the ink can easily transfer from tip to the substrate upon contact, which forms a lattice consisted of hemispherical dots with nearly 2 μm diameter of each dot (Fig. 4(b)). Unfortunately, such small contact angle facilitates excessive amount of ink transfer from the tip to the substrate, which makes it difficult for not only precise confinement of sizes of patterned dots, but also coarsening of the dot arrays through annealing treatment. This finally leads to formation of multiple crystal nuclei instead of single NP [33].

Reversely, if the surface is too hydrophobic, ink transfer may become highly impossible and no pattern can be obtained. As shown in Fig. 4(c), ethanol-based ink could not form continuous droplets and no pattern was seen after treatment of the substrate by immersing into the ethanol solution of perfluorododecyltrichlorosilane after surface plasma bombardment, which leads to contact angle of 108° (Fig. 4(d)). Systematic investigations suggested that treatment of the substrate by ethanol solution of hexamethyldisilane (HMDS) results in a moderate contact angle of 70°–90° (Fig. 4(e)). At this time, not only the regular and uniform arrays could be reliably printed on the substrate, patterns of individual UCNPs can be obtained after further coarsening of such polymeric nanoreactor arrays through annealing treatment (Fig. 4(f)). Therefore, as long as the substrate contact angle is between 70°–90°, in addition to quartz, such dot arrays could also be generated on silicon substrates (Figs. S3 and S4 in the ESM).

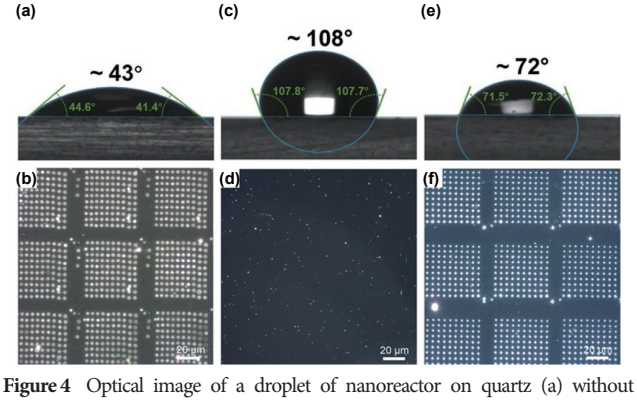

Figure 4 Optical image of a droplet of nanoreactor on quartz (a) without surface treatment showing low contact angle, and treated with (c) perfluorodecyl trichlorosilane and (e) HMDS. (b), (d), and (f) are corresponding dark-field optical microscope images of the nanoreactor arrays generated by PPL under the condition of (a), (c), and (e), respectively.

The next challenge to convert such-generated PEG dot arrays containing expected RE^{3+} ions at predesigned molar ratios is to slowly remove the organic component such as PEG, ethanol, and PVP (or oleic acid) by heating in the air, where proper annealing parameters, such as heating rate, temperature, and annealing time, are especially important. If the temperature is too low, organic component could not be completely burned out and poor crystallinity of particles will be obtained, which leads to poor luminescent performance (Figs. 5(a) and 5(b)). If the heating rate is too high, coarsening becomes aboil and multiple nuclei will be generated (Figs. 5(c) and 5(d)).

Further investigations have indicated that at proper temperature with moderate heating rate and suitable annealing time, arrays containing high quality UCNP reflected by the strong luminescence signal can be reliably generated, and meanwhile the organic component can be completely removed, as shown by the optical and scanning electron microscopic (SEM) images in Figs. 6(a)–6(c). The optical properties of UCNP arrays were investigated using a home-built optical microscopy and spectroscopy system (Fig. S5 in the ESM). As a representative, the laser-scanning microscopic images and luminescence spectrum of the dot array of Y_2O_3:Yb/Ho (20/1 mol%) were successfully collected (Figs. 6(d)–6(f) and Fig. S6 in the ESM) [34].

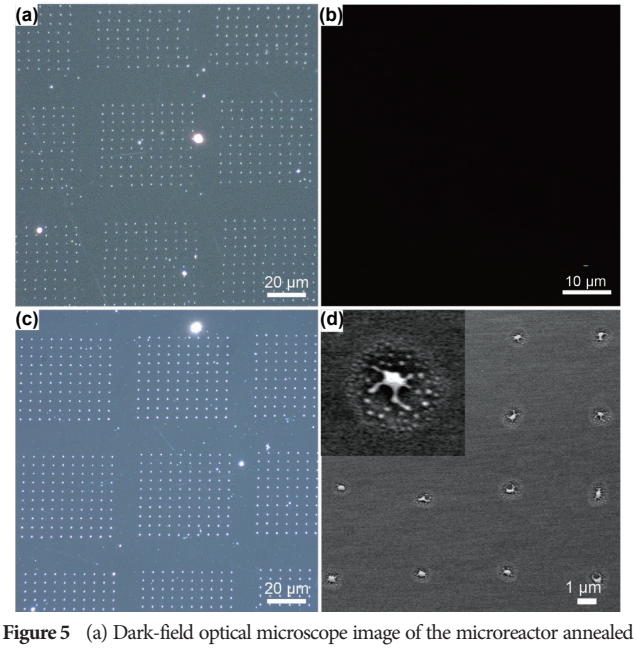

Figure 5 (a) Dark-field optical microscope image of the microreactor annealed at low temperature. (b) Fluorescent image of patterned UCNPs doped with Yb^{3+} and Ho^{3+} detected through the green channel. (c) Dark-field optical microscope image of the microreactor after annealing. (d) SEM images of UCNP arrays showing in (c).

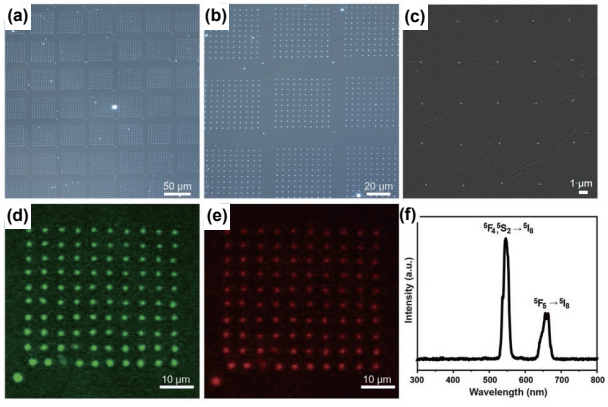

Figure 6 Dark field optical microscope images of the microreactor array after annealing at (a) low and (b) high magnification. (c) SEM image of UCNP array seen in (b). Fluorescent images of UCNP arrays doped with Yb^{3+}/Ho^{3+} collected by (d) green and (e) red channels. (f) Emission spectrum of UCNP array under 980 nm laser excitation.

3 Conclusions

In summary, we have developed a simple and efficient ink preparation method and achieved large-area and 100% repeatable printing of UCNP arrays, which also works for different substrates. This work overcomes the long-standing problem of printing ionic substances through PPL and controllable synthesis of uniform NP arrays. The strategy reported has made possible for exploring functionalities of more ionic species, understanding the nanoscaled chemistry, as well as designing multiplexed and multifunctional nanoarrays.

4 Experimental section

4.1 Materials

Lanthanide nitrate ($Y(NO_3)_3$, $Yb(NO_3)_3$, $Er(NO_3)_3$, $Ho(NO_3)_3$, $Tm(NO_3)_3$), were purchased from Sinopharm Chemical Reagent, Co., Ltd. (Beijing, China). Polyethylene glycol 400 ($Ho(CH_2CH_2O)H$, 99%), ethanol (C_2H_6O, AR), acetone (C_3H_6O, AR), isopropanol (C_3H_8O, AR), methanol (C_2H_5OH, AR), and toluene (C_7H_8, AR) were purchased from Shanghai Lingfeng Chemical Reagent Co., Ltd. (Shanghai, China). Polyvinyl pyrrolidone ($(C_6H_9NO)_n$, M_W = 40,000), and 1H,1H,2H,2H-perfluorodecyltrichlorosilane ($C_{10}H_4Cl_3F_{17}Si$, 98%) were purchased from Sigma-Aldrich. 1,1,1,3,3,3-Hexamethyldisilazane ($C_6H_{19}NSi_2$, 99%) were purchased from Energy Chemical. All reagents and solvents were used as received without any further purification.

4.2 Ink preparation and loading

Rare earth nitrates and PVP (M_W = 40,000) were added to an ethanol solution of PEG-400. The concentration of rare earth nitrate was 20 mM, the amount of added PVP was 5 mg/mL, and the amount of added PEG-400 was 10 μL/mL. After ultrasound for 5 min, the rare earth ions and polymer mixture were drip-coated on PPL pen arrays, which was then used for lithography.

4.3 Constructing microreactors by polymer pen lithography

Quartz substrates were modified overnight by enclosure in a chamber with vials containing a HMDS/toluene mixture (volume ratio = 1:4). PDMS pen arrays were fabricated following a published protocol [35]. The pen array was treated by oxygen plasma and drip-coated with the ink, then loaded onto the desktop nanopatterning instrument (TERA-print M series) and leveled to be parallel with the substrate. Finally, the pen arrays contacted with the substrate, and extended a certain length (extension length, LE) to form nanoreactors.

4.4 Coarsening and annealing treatment

The substrate was heat treated in the muffle furnace in ambient air. The progresses were in detail as follow: ramp to 120 °C for 12 h, cool down to room temperature in 1 h, ramp to 1,000 °C in 200 min, hold at 1,000 °C for 8 h, and cool down to room temperature in 3 h.

4.5 Characterization

Microreactor arrays and upconversion nanoparticle arrays were imaged using an optical microscope (Nikon LV100ND) under dark-field (DF) conditions with a halogen light source. The morphology of the upconversion nanoparticle arrays was characterized by SEM (JEOL, JSM-7800F) equipped with a cold field emission gun (cFEG) operated at 1 to 15 kV. FT-IR spectral data were obtained from a Nicolet iS10 FT-IR spectrometer. Powder X-ray diffraction (XRD) data were recorded on a Rigaku D/max 2550 X-ray diffractometer with Cu Kα radiation (λ = 1.5406 Å).

A laboratory-fabricated optical system was established to achieve laser scanning fluorescence imaging of Y_2O_3:Yb/Ho (20/1 mol%) nanoparticles by using a 975 nm continuous-wave single-mode diode laser (Laser 1, B&A Technologies Co., Ltd.) and a commercial multi-photon laser scanning microscope (FV1000MPE-S with motorized inverted IX81, Olympus). The microscope was equipped with a galvanoscope scanning unit and a non-descanned detection (NDD) module, in which two high-sensitivity photo-multiplier tubes (PMT) were used as single-photon counting detectors for green and red color fluorescence imaging. After the laser beam entered the microscope and was reflected by 690 nm short-pass dichroism mirror, it was focused on the sample by oil-immersed objective lens (OL, 100×/NA = 1.45, UPLXAPO100XO, Olympus). Fluorescence was collected through the same objective, filtered through a 690-nm short-pass dichroic mirror, and finally detected by the PMTs. A 720 nm short-pass filter (FF01-720/SP-25, used by Semrock) was installed in the PMTs to further block the laser light, and then the green and red upconversion emissions were filtered with a 550 nm band-pass filter (ET550/20×, Chroma) and a 660 nm band-pass filter (FF01-660/30-25, Semrock), respectively.

Acknowledgements

The work reported here was supported by the Major Research Program Cultivation Project of National Science Foundation of China (No. 91956107) and the National Natural Science Foundation of China (Nos. 2201101389, 21871137, 62122028, and 11974123).

Electronic Supplementary Material: Supplementary material (optical microscope images of the nanoreactors arrays containing different ionic components in PEG ethanol solution and on different substrates, working mechanism of the home-built optical system used for scanning the dot arrays of Y_2O_3:Yb/Ho, and XRD patterns of Y_2O_3:Yb/Ho samples) is available in the online version of this article at https://doi.org/10.1007/s12274-022-4968-0.

References

[1] Kar, A.; Patra, A. Impacts of core–shell structures on properties of lanthanide-based nanocrystals: Crystal phase, lattice strain, downconversion, upconversion and energy transfer. *Nanoscale* **2012**,

4, 3608–3619.
[2] Haase, M.; Schäfer, H. Upconverting nanoparticles. *Angew. Chem., Int. Ed.* **2011**, *50*, 5808–5829.
[3] Gorris, H. H.; Wolfbeis, O. S. Photon-upconverting nanoparticles for optical encoding and multiplexing of cells, biomolecules, and microspheres. *Angew. Chem., Int. Ed.* **2013**, *52*, 3584–3600.
[4] Tian, G.; Gu, Z. J.; Zhou, L. J.; Yin, W. Y.; Liu, X. X.; Yan, L.; Jin, S.; Ren, W. L.; Xing, G. M.; Li, S. J. et al. Mn^{2+} dopant-controlled synthesis of $NaYF_4$:Yb/Er upconversion nanoparticles for *in vivo* imaging and drug delivery. *Adv. Mater.* **2012**, *24*, 1226–1231.
[5] Auzel, F. Upconversion and anti-stokes processes with f and d ions in solids. *Chem. Rev.* **2004**, *104*, 139–174.
[6] Downing, E.; Hesselink, L.; Ralston, J.; Macfarlane, R. A three-color, solid-state, three-dimensional display. *Science* **1996**, *273*, 1185–1189.
[7] Xie, H. B.; Zhang, J. N.; Wang, F.; Shen, D. Y.; Wang, J.; Tang, D. Y. High-power 1,640 nm Er:Y_2O_3 ceramic laser at room temperature. *Opt. Lett.* **2022**, *47*, 246–248.
[8] Sun, L. D.; Dong, H.; Zhang, P. Z.; Yan, C. H. Upconversion of rare earth nanomaterials. *Annu. Rev. Phys. Chem.* **2015**, *66*, 619–642.
[9] Zhang, H. X.; Chen, Z. H.; Liu, X.; Zhang, F. A mini-review on recent progress of new sensitizers for luminescence of lanthanide doped nanomaterials. *Nano Res.* **2020**, *13*, 1795–1809.
[10] Kostyuk, A. B.; Vorotnov, A. D.; Ivanov, A. V.; Volovetskiy, A. B.; Kruglov, A. V.; Sencha, L. M.; Liang, L. E.; Guryev, E. L.; Vodeneev, V. A.; Deyev, S. M. et al. Resolution and contrast enhancement of laser-scanning multiphoton microscopy using thulium-doped upconversion nanoparticles. *Nano Res.* **2019**, *12*, 2933–2940.
[11] Mor, F. M.; Sienkiewicz, A.; Forró, L.; Jeney, S. Upconversion particle as a local luminescent Brownian probe: A photonic force microscopy study. *ACS Photonics* **2014**, *1*, 1251–1257.
[12] Lu, Y. Q.; Zhao, J. B.; Zhang, R.; Liu, Y. J.; Liu, D. M.; Goldys, E. M.; Yang, X. S.; Xi, P.; Sunna, A.; Lu, J. et al. Tunable lifetime multiplexing using luminescent nanocrystals. *Nat. Photonics* **2014**, *8*, 32–36.
[13] You, W. W.; Tu, D. T.; Li, R. F.; Zheng, W.; Chen, X. Y. "Chameleon-like" optical behavior of lanthanide-doped fluoride nanoplates for multilevel anti-counterfeiting applications. *Nano Res.* **2019**, *12*, 1417–1422.
[14] Hartman, T.; Geitenbeek, R. G.; Whiting, G. T.; Weckhuysen, B. M. *Operando* monitoring of temperature and active species at the single catalyst particle level. *Nat. Catal.* **2019**, *2*, 986–996.
[15] Xie, S. T.; Du, Y. L.; Zhang, Y.; Wang, Z. M.; Zhang, D. L.; He, L.; Qiu, L. P.; Jiang, J. H.; Tan, W. H. Aptamer-based optical manipulation of protein subcellular localization in cells. *Nat. Commun.* **2020**, *11*, 1347.
[16] Ke, J. X.; Lu, S.; Li, Z.; Shang, X. Y.; Li, X. J.; Li, R. F.; Tu, D. T.; Chen, Z.; Chen, X. Y. Multiplexed intracellular detection based on dual-excitation/dual-emission upconversion nanoprobes. *Nano Res.* **2020**, *13*, 1955–1961.
[17] Chen, S.; Weitemier, A. Z.; Zeng, X.; He, L. M.; Wang, X. Y.; Tao, Y. Q.; Huang, A. J. Y.; Hashimotodani, Y.; Kano, M.; Iwasaki, H. et al. Near-infrared deep brain stimulation via upconversion nanoparticle-mediated optogenetics. *Science* **2018**, *359*, 679–684.
[18] Richards, B. S.; Hudry, D.; Busko, D.; Turshatov, A.; Howard, I. A. Photon upconversion for photovoltaics and photocatalysis: A critical review. *Chem. Rev.* **2021**, *121*, 9165–9195.
[19] Liu, X. Y.; Liu, W. D.; Yang, B. Deep-elliptical-silver-nanowell arrays (d-EAgNWAs) fabricated by stretchable imprinting combining colloidal lithography: A highly sensitive plasmonic sensing platform. *Nano Res.* **2019**, *12*, 845–853.
[20] Bhingardive, V.; Menahem, L.; Schvartzman, M. Soft thermal nanoimprint lithography using a nanocomposite mold. *Nano Res.* **2018**, *11*, 2705–2714.
[21] Williams, G.; Hunt, M.; Boehm, B.; May, A.; Taverne, M.; Ho, D.; Giblin, S.; Read, D.; Rarity, J.; Allenspach, R. et al. Two-photon lithography for 3D magnetic nanostructure fabrication. *Nano Res.* **2017**, *11*, 845–854.
[22] Piner, R. D.; Zhu, J.; Xu, F.; Hong, S.; Mirkin, C. A. "Dip-pen" nanolithography. *Science* **1999**, *283*, 661–663.
[23] Demers, L. M.; Ginger, D. S.; Park, S. J.; Li, Z.; Chung, S. W.; Mirkin, C. A. Direct patterning of modified oligonucleotides on metals and insulators by dip-pen nanolithography. *Science* **2002**, *296*, 1836–1838.
[24] Lim, J. H.; Ginger, D. S.; Lee, K. B.; Heo, J.; Nam, J. M.; Mirkin, C. A. Direct-write dip-pen nanolithography of proteins on modified silicon oxide surfaces. *Angew. Chem., Int. Ed.* **2003**, *42*, 2309–2312.
[25] Huang, L.; Braunschweig, A. B.; Shim, W.; Qin, L. D.; Lim, J. K.; Hurst, S. J.; Huo, F. W.; Xue, C.; Jang, J. W.; Mirkin, C. A. Matrix-assisted dip-pen nanolithography and polymer pen lithography. *Small* **2010**, *6*, 1077–1081.
[26] Du, J. S.; Chen, P. C.; Meckes, B.; Kluender, E. J.; Xie, Z.; Dravid, V. P.; Mirkin, C. A. Windowless observation of evaporation-induced coarsening of Au-Pt nanoparticles in polymer nanoreactors. *J. Am. Chem. Soc.* **2018**, *140*, 7213–7221.
[27] Qin, L. D.; Park, S.; Huang, L.; Mirkin, C. A. On-wire lithography. *Science* **2005**, *309*, 113–115.
[28] Sanedrin, R. G.; Huang, L.; Jang, J. W.; Kakkassery, J.; Mirkin, C. A. Polyethylene glycol as a novel resist and sacrificial material for generating positive and negative nanostructures. *Small* **2008**, *4*, 920–924.
[29] Chai, J. N.; Huo, F. W.; Zheng, Z. J.; Giam, L. R.; Shim, W.; Mirkin, C. A. Scanning probe block copolymer lithography. *Proc. Natl. Acad. Sci. USA* **2010**, *107*, 20202–20206.
[30] Chen, P. C.; Liu, X. L.; Hedrick, J. L.; Xie, Z.; Wang, S. Z.; Lin, Q. Y.; Hersam, M. C.; Dravid, V. P.; Mirkin, C. A. Polyelemental nanoparticle libraries. *Science* **2016**, *352*, 1565–1569.
[31] Ali, F. M.; Kershi, R. M. Synthesis and characterization of La^{3+} ions incorporated (PVA/PVP) polymer composite films for optoelectronics devices. *J. Mater. Sci. Mater. Electron.* **2020**, *31*, 2557–2566.
[32] Kumar, B.; Kaur, G.; Rai, S. B. Sensitized green emission of terbium with dibenzoylmethane and 1,10-phenanthroline in polyvinyl alcohol and polyvinyl pyrrolidone blends. *Spectrochim. Acta A Mol. Biomol. Spectrosc.* **2017**, *187*, 75–81.
[33] Chai, J. N.; Liao, X.; Giam, L. R.; Mirkin, C. A. Nanoreactors for studying single nanoparticle coarsening. *J. Am. Chem. Soc.* **2012**, *134*, 158–161.
[34] Xing, M. M.; Cao, W. H.; Zhong, H. Y.; Zhang, Y. H.; Luo, X. X.; Fu, Y.; Feng, W.; Pang, T.; Yang, X. F. Synthesis and upconversion luminescence properties of monodisperse Y_2O_3: Yb, Ho spherical particles. *J. Alloys Compd.* **2011**, *509*, 5725–5730.
[35] Eichelsdoerfer, D. J.; Liao, X.; Cabezas, M. D.; Morris, W.; Radha, B.; Brown, K. A.; Giam, L. R.; Braunschweig, A. B.; Mirkin, C. A. Large-area molecular patterning with polymer pen lithography. *Nat. Protoc.* **2013**, *8*, 2548–2560.